




# In-situ SEM study of temperature-dependent tensile behavior of Inconel 718 superalloy

Lijun Sang<sup>1</sup>, Junxia Lu<sup>1,\*</sup>, Jin Wang<sup>2</sup>, Rafi Ullah<sup>1</sup>, Xiangcheng Sun<sup>3</sup>, Yuefei Zhang<sup>1,\*</sup> , and Ze Zhang<sup>2</sup>

<sup>1</sup> Faculty of Materials and Manufacturing, Beijing University of Technology, Beijing 100124, China

<sup>2</sup> School of Materials Science and Engineering, Zhejiang University, Hangzhou 310027, China

<sup>3</sup> Institute of Science and Technology, Yantai Nanshan University, Yantai 265700, China

Received: 15 March 2021

Accepted: 9 June 2021

Published online:

12 July 2021

© The Author(s), under exclusive licence to Springer Science+Business Media, LLC, part of Springer Nature 2021

## ABSTRACT

The effect of deformation temperature on tensile behavior of Inconel 718 alloy has been studied by a self-developed in-situ high-temperature tensile stage inside a scanning electron microscopy at a temperature range from room temperature (RT) to 750 °C. The dynamic microstructure evolution and mechanical properties at different temperatures were performed and compared by the uniaxial tensile tests. The in-situ test results showed that the mechanical properties and fracture mechanisms of Inconel 718 alloy were sensitive to deformation temperatures. From RT to 650 °C, the yield stress and ultimate tensile strength decrease slightly and the tensile ductility is comparable. While up to 750 °C, the yield stress and ultimate tensile strength decrease significantly, the elongation and reduction of cross section also showed a significant decrease from RT to 750 °C. It was found that at RT and 650 °C, tensile cracks tended to initiate around the carbide particles and the triple junctions of grain boundaries, also propagated transgranularly; at 750 °C, the cracks initiated at grain boundaries and propagated intergranularly. In fact, with the increase in deformation temperature, the fracture mechanism transformed from the ductile transgranular fracture to the brittle intergranular fracture.

## Introduction

Inconel 718 (IN718) has excellent cyclic fatigue resistance, high tensile strength, good corrosion resistance and oxidation resistance at elevated

temperature [1, 2]. Thus, it is widely used in aerospace field for manufacturing of critical components, such as combustion chambers, aircraft turbine disks, shafts, fasteners, guide vanes. [3, 4]. IN718 alloy is a typical precipitate-strengthened nickel-based superalloy with face-centered cubic (fcc) structure. The

Handling Editor: Sophie Primig.

Address correspondence to E-mail: junxialv@bjut.edu.cn; yfzhang@bjut.edu.cn

E-mail Addresses: sanglijun@bigc.edu.cn; wangjinjz008@emails.bjut.edu.cn; rafi\_hassan2011@yahoo.com; sunxc824@163.com; zezhang@zju.edu.cn

<https://doi.org/10.1007/s10853-021-06256-8>

strength at elevated temperature is primarily derived from metastable  $\gamma''$  phase ( $\text{Ni}_3\text{Nb}$  based  $\text{D0}_{22}$  structure) coupled with a small amount of spherical  $\gamma'$  phase ( $\text{Ni}_3\text{Al}$  based  $\text{L1}_2$  structure) and carbides [5–8]. Therein,  $\gamma''$  phase has a good coherent relationship with the  $\gamma$  matrix and its size and quantity will directly decide the comprehensive mechanical properties of the alloy. However, during long-time service at high-temperature or heat treatment,  $\gamma''$  phase is unstable and prone to transform into the incoherent equilibrium phase  $\delta$  ( $\text{Ni}_3\text{Nb}$  based  $\text{D0}_a$  structure), which can stably exist at elevated temperature and decrease the strength of the alloy [9–11].

As an aero-engine structural material, IN718 alloy is simultaneously subjected to high temperature and high stress during a long-term service, resulting in a continuous evolution of microstructures of the alloy. The evolution of microstructure directly affects the mechanical properties of materials [12–14]. Thus, it is necessary to study the dynamic relationship between the microstructure evolution and variation of mechanical properties of IN718 alloy under conditions of changing temperature and stress, which is helpful to understand the fracture mechanism of IN718 alloy under similar service conditions. Some investigations have been carried out to study deformation behaviors and the structure–property relationships of IN718 alloy at different temperatures. Liu et al. [15] studied the effect of grain size on the fracture behavior during uniaxial tensile tests performed on IN718 sheets at room temperature, and explained the fracture behavior with respect to the influence of the microstructure, but the effect of tensile temperature on the fracture behavior was neglected. Wang et al. [16] studied the hot deformation behaviors of IN718 alloy at elevated temperatures ranging from 950 to 1050 °C by ex-situ tensile tests, and found that dynamic recrystallization is responsible for the flow oscillations in stress at lower strain rates. Lin et al. [17] studied the effects of deformation temperature and strain rate on the fracture morphology of IN718 by ex-situ hot uniaxial tensile tests at the temperature ranging from 920 to 1040 °C and strain rate range of 0.001–0.01  $\text{s}^{-1}$ , and found that the flow behaviors are significantly affected by the deformation temperature, strain and strain rate. Zhao et al. [18] studied the influence of the grain size and strain rate on fracture behaviors of IN718 thin sheets using ex-situ uniaxial tensile tests at 800 °C, and proposed a two-step fracture mechanism

based on the post-mortem observation of fracture morphology by SEM. Lu et al. [19] investigated the high-temperature tension and low cycle fatigue deformation behaviors of IN718 alloy in the electro-hydraulic servo system with SEM at 455 °C, and found that the carbide and twin grain are the crack source during the low cycle fatigue. The fatigue crack initiation and propagation were observed in situ, but the detailed microstructure evolution and fracture behavior until failure were scarcely mentioned in the article.

Though plenty of tensile deformation behaviors of IN718 alloy at high temperature were studied, the experiments were mainly conducted by ex-situ tensile tests. Fracture mechanisms are mostly deduced from the speculation of the fracture process by observing fractographies. Only a few in-situ researches are based on room temperature or a far lower temperature than that service temperature of IN718 alloy [19–21]. Therefore, in-situ comparison of the microstructure evolution and the whole fracture process during tensile tests at room temperature and elevated temperature is of great significance, which will greatly help to understand the effects of deformation temperature on fracture mechanism of IN718 alloy.

In this study, the effect of deformation temperature on the mechanical properties of IN718 alloy were studied at room temperature (RT), 650 °C and 750 °C using uniaxial tensile tests. The crack initiation and propagation process were observed via real-time observation of the microstructural evolution behaviors by putting the tensile stage into SEM chamber. The fracture surfaces were also characterized by SEM after tensile tests. Based on the experimental results, the effects of deformation temperature on mechanical properties and deformation mechanism were discussed. The experimental results would be of importance to better clarify the structure–property relationship and fracture mechanism for the superalloy at different temperatures.

## Experimental material and procedures

### Specimen preparation

The hot-rolled bars with 30 mm in diameter of IN718 alloy were used in this study. The chemical compositions (in wt%) of the alloy are shown in Table 1. The

bars were firstly subjected to a heat treatment procedure consisting of a solution heat treatment at 1050 °C for 1 h followed by water quenching. Then, the bars were aged at 725 °C for 15 h followed by air quenching.

The tensile specimens were wire-cut into the double-dog bone geometry with a gage length of 2 mm, a gage width of 1 mm, and a gage thickness of 0.7 mm. The machining dimensions are shown in Fig. 1. The ladder shape was prone to form the stress concentration area, where the microstructure evolution, as well as the crack initiation and propagation were observed in situ during the high-temperature tensile tests. To reveal the prevailing microstructure of the specimens via SEM, the specimens were firstly prepared using typical metallographic grinding and polishing techniques with SiC abrasive papers (from 400 to 2000 grit) until mirror smooth. The specimens were then etched chemically with a mixture solution of 5 g  $\text{CuCl}_2$ , 100 ml HCl, and 100 ml  $\text{C}_2\text{H}_5\text{OH}$  for approx. 1 min at room temperature.

### In-situ tensile tests

The in-situ tensile testing system developed by the authors has been integrated into a FEI Quanta650 FEG SEM, as shown in Fig. 2a. The design allows for the stage to be mounted inside a SEM, thus allowing high-resolution and time-resolved observations to be carried out. The system integrates both tensile stage and the heater for high-temperature tensile work all together. The schematic diagram of heater and clamps is shown in Fig. 2b. The left and right clamps are controlled by a multistep gear-drive system, which can achieve the axisymmetric uniaxial bidirectional tension. The heating core with a diameter of 8 mm slightly touches the testing specimen to heat it by conduction mode. A K-type thermocouple is used to monitor the temperature by contacting with the lower surface of the specimen. The tensile system can provide a maximum load of 2224 N and a maximum displacement of 40 mm at a temperature range up to 900 °C. A detailed description of the device has been reported in previous work [22].

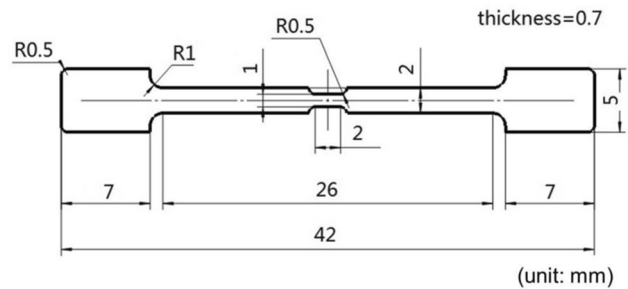


**Figure 1** Dimensions of the in-situ tensile specimen.

The in-situ uniaxial tensile tests were conducted at a displacement rate of 0.5  $\mu\text{m/s}$  and at RT, 650 °C and 750 °C until failure. At each temperature, five specimens were subjected to tensile testing to calculate the average mechanical properties of IN718 alloy. Before tensile test, the size of specimens was measured again in order to confirm the effective cross section, due to the reduction effect of the polishing. Subsequently, the specimen was heated to the selected testing temperature step by step and held for 30 min to ensure temperature uniformity along the gage section. The tensile load–displacement curve was recorded in real-time via the control system. The corresponding stress is obtained by the load divided by the effective cross-section area. In-situ SEM images were taken at pauses in the tensile process. After image acquisition, the test was resumed using identical displacement-controlled conditions.

## Results

### The initial microstructures

The initial microstructure of IN718 alloy before tensile tests was observed through SEM and the results are shown in Fig. 3. It can be found that the grains are equiaxed with the average size of about 95  $\mu\text{m}$ . In addition, lamella-like twins formed during annealing are also distributed in the matrix. By local magnification, some polygonal-shaped particles embedded inside matrix (marked by yellow arrows) can be seen in Fig. 3b, which were confirmed to be (Nb, Ti)C carbides and (Ti, Nb)(C,N) carbonitrides according to

**Table 1** Chemical compositions of IN718 alloy (wt%)

Ni	Cr	Fe	Mo	C	Co	W	Mn	Nb	V	Al	Ti
52.99	17.3	19.36	3.52	0.07	0.01	0.08	0.05	5.26	0.01	0.52	0.83

**Figure 2** **a** In-situ high-temperature tensile stage positioned inside the SEM chamber; **b** schematic diagram of the main working parts.

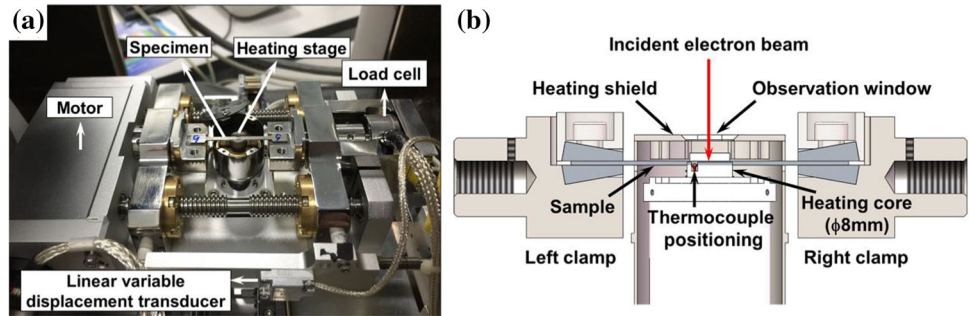
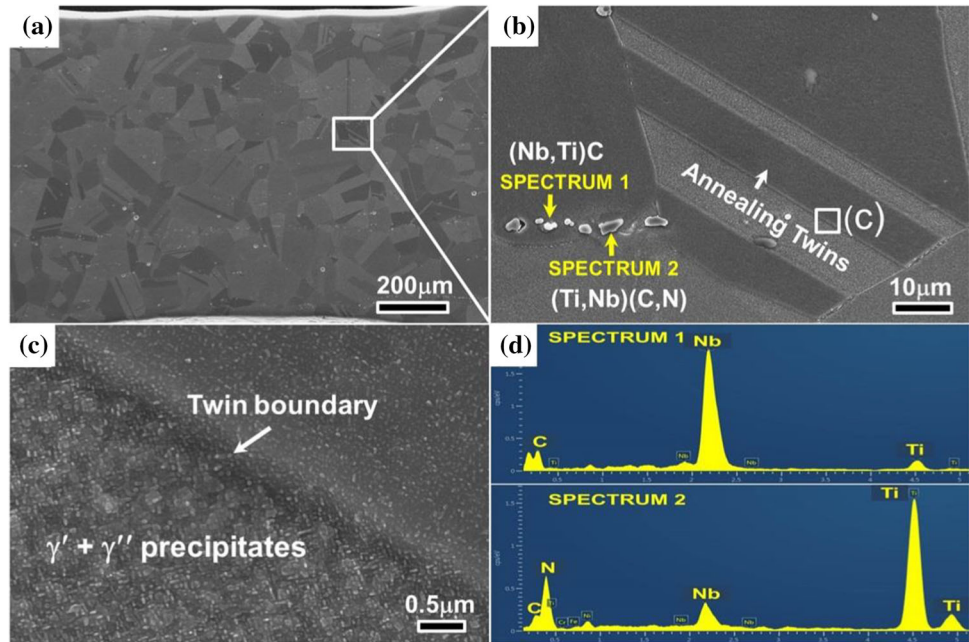


**Figure 3** SEM images of the initial microstructure of IN718 alloy: **a** grain distribution; **b** higher magnification of the marked region in (a); **c** enlarged image of the region marked as c in (b); **d** EDS spectrums of carbide and carbonitride in (b).



Energy Dispersive Spectroscopy (EDS) analysis, as shown in Fig. 3d. Along the twin grain boundary (marked as c in Fig. 3b) nano-sized  $\gamma'$ / $\gamma''$  precipitates was identified in the microstructure of  $\gamma$  matrix, as shown in Fig. 3c. The  $\delta$  phase was not observed in the microstructure. This indicated that the  $\delta$  phase was completely dissolved during the heat treatment.

### Tensile properties

In order to compare the influence of temperature on microstructure and mechanical properties, subsequently in-situ tensile experiments were done. Typical tensile stress–strain curves at RT, 650 °C and 750 °C are shown in Fig. 4, respectively. It is worth noting that the appearance of stepwise patterns in curves is mainly due to the stress relaxation and the intermittent starting and stopping during the tensile tests [23]. Such phenomenon is particularly evident at 750

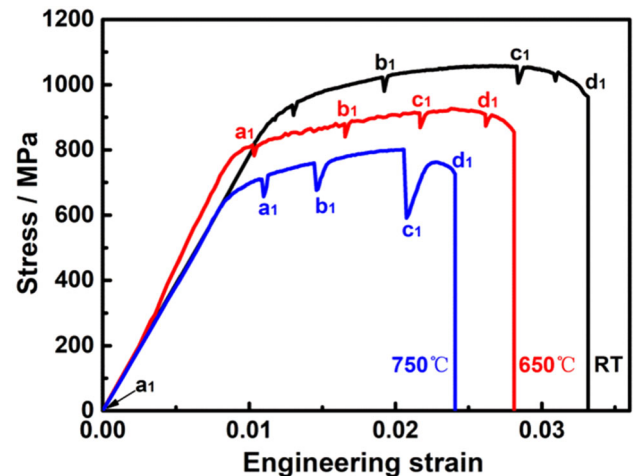


**Figure 4** Engineering stress–strain curves measured during the in-situ tensile tests at RT, 650 °C and 750 °C.

°C due to the thermal softening. The strain hardening phenomenon was observed after yielding in all

curves. The average values of yield stress (YS), ultimate tensile strength (UTS), elongation to fracture and reduction of cross section are tabulated in Table 2. The corresponding standard deviations are also shown in parentheses in Table 2. It can be found that all the values decrease with the increase of temperature.

From RT to 650 °C, the YS and UTS decreased by 60 MPa and 131 MPa. In contrast, the YS and UTS decreased by 200 MPa and 257 MPa from RT to 750 °C. It revealed that the mechanical properties decrease significantly at 750 °C. Notably, the elongation to failure and reduction of cross section from RT to 750 °C decreased significantly from 43.1 to 31.3% and from 38.5 to 12.5%, respectively. The similar results were also observed and the reason is ascribed to some alloy elements, such as O, S, C, Cr segregation to grain boundary, which finally induced the ductility decrease and caused the intermediate temperature embrittlement [24, 25].

### In-situ observations of tensile deformation behavior at RT, 650 °C and 750 °C

In-situ SEM observations reveal that the surface morphology changes accordingly during sequential tensile tests at different temperatures.

Figure 5 shows the whole deformation process and the microstructure evolution under uniaxial tension at RT. Figure 5a1 and a2 shows the original smooth and flat surface before applying of tensile load. When the strain reached 0.019 (point  $b_1$  on the black line in Fig. 4), the surface of specimen became undulated shown in Fig. 5b1. Close examination reveals that the deformation is accommodated by crystal slip. This is evidenced by the direct observation of slip lines formation and stretching of grains on the surface of specimen in Fig. 5b2. With increasing strain to 0.028 (point  $c_1$  on the black line in Fig. 4), the necking behavior and a wrinkled surface became apparent as

shown in Fig. 5c1. In particular, the density of present slip bands is shown to grow and voids are found in the vicinity of carbides shown in Fig. 5c2. It is worth noting that some carbides have cracked and the formation of these voids is caused by the debonding at the interface of  $\gamma$  matrix and carbides. Figure 5d1 and d2 shows that the fracture is a transgranular mode. The fracture path is almost perpendicular to the external tensile load. The longitudinal length decreases from 888 to 622  $\mu\text{m}$ , and the longitudinal strain is up to 30%. In a word, the necking is very obvious.

Figure 6 shows the whole deformation process, including the crack initiation and propagation under uniaxial tension at 650 °C. It is apparent that the behavior at this temperature is broadly similar to that at RT. When the stress reached the yield limit (point  $a_1$  on the red line in Fig. 4), plastic deformation occurred by crystal slip and multiple slip lines were observed in Fig. 6a2 due to the thermal activity. As the strain increased to 0.016 (point  $b_1$  on the red line in Fig. 4), the necking occurred and voids were observed on the surface of necking region shown in Fig. 6b1 and b2. With the strain further increasing, two cracks were observed at the strain about 0.021 (point  $c_1$  on the red line in Fig. 4), as shown in Fig. 6c1 and c2. As the stress reached UTS and then dropped to 909 MPa (point  $d_1$  on the red line in Fig. 4), two cracks propagated in a transgranular manner and were inclined to coalesce at strain about 0.026, as shown in Fig. 6d1 and d2. The longitudinal length decreases from 877 to 752  $\mu\text{m}$ , and the longitudinal strain is about 14%. Therefore, the necking became less apparent than that at RT, which indicated that the stress concentration was partially released.

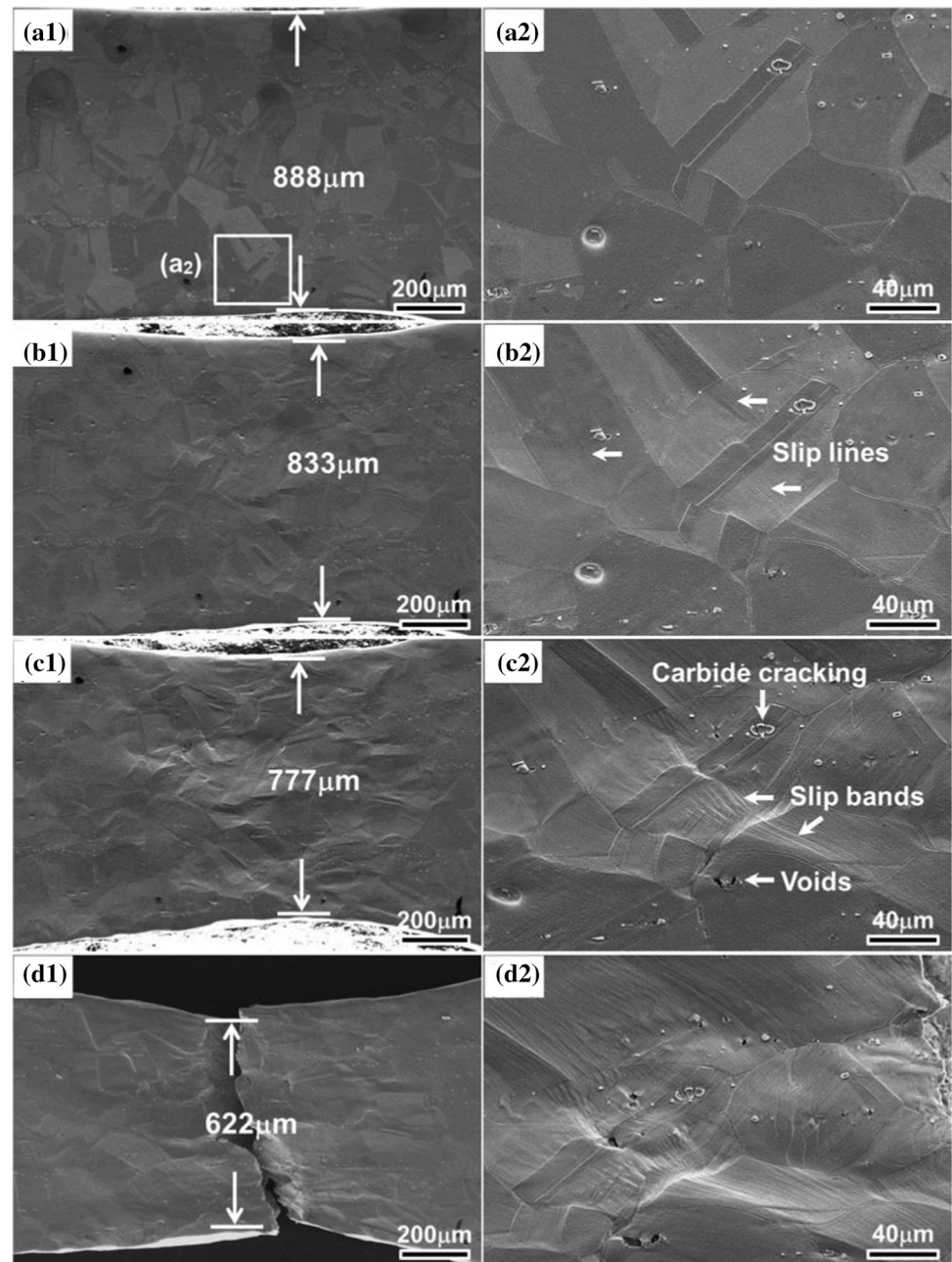
Figure 7 shows the SEM micrographs of microstructures for the specimen tested at 750 °C under different strain levels. The deformation behavior at 750 °C is distinguished from that one

**Table 2** Tensile properties of IN718 alloy at RT, 650 °C and 750 °C

Test temperature (°C)	Yield stress (MPa)	Ultimate tensile strength (MPa)	Elongation (%)	Reduction of cross section (%)
RT	862 (3.4)	1057 (4.9)	43.1 (2.6)	38.5 (1.5)
650	802 (3.2)	926 (3.5)	36.6 (1.3)	28.2 (0.8)
750	662 (6.6)	800 (5.7)	31.3 (1.5)	12.5 (1.9)

The values in parentheses are standard deviations

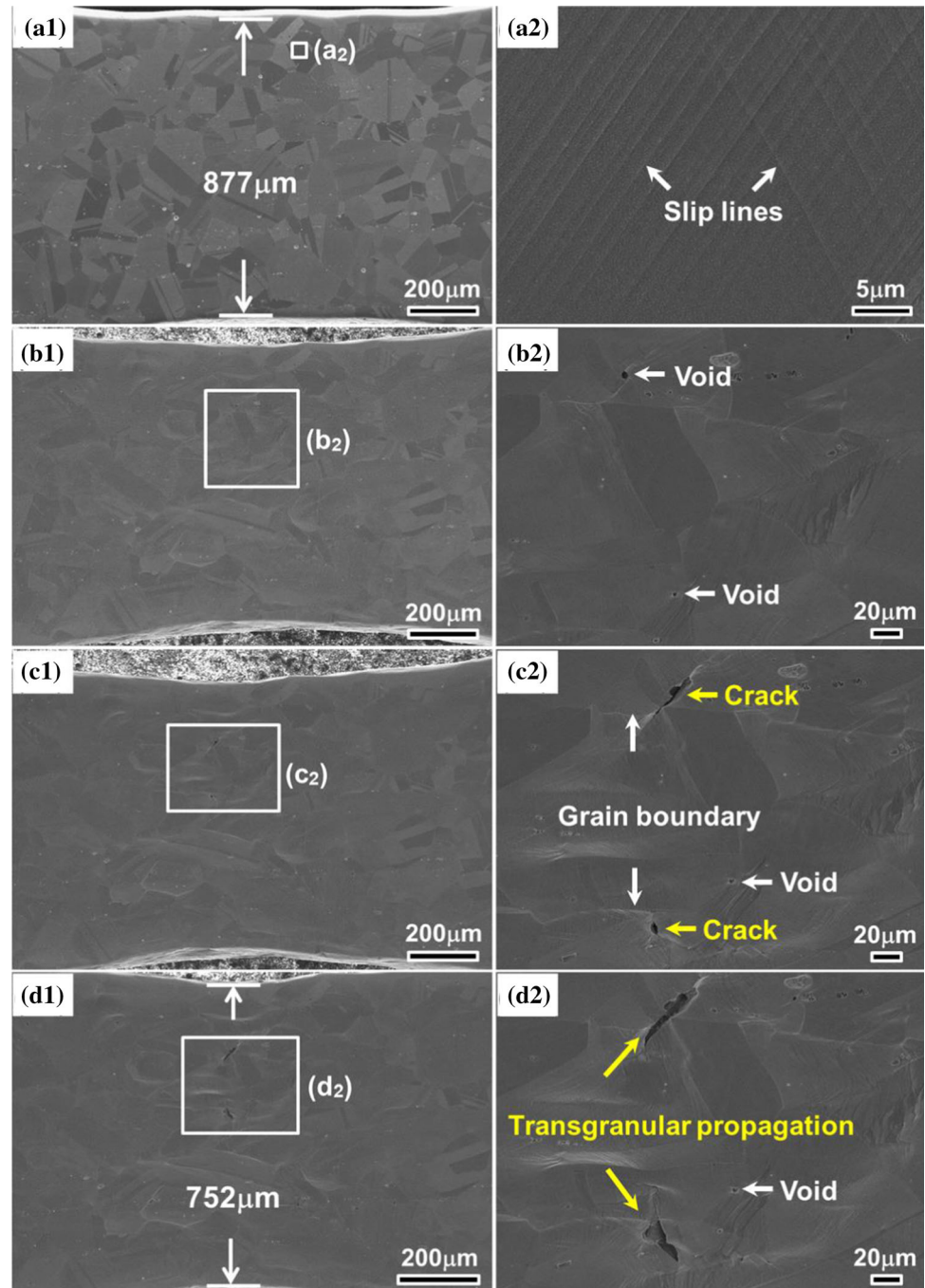
**Figure 5** In-situ tensile deformation process at RT under strain levels: ( $a_1 - a_2$ ) 0, ( $b_1 - b_2$ ) 0.019, ( $c_1 - c_2$ ) 0.028, and ( $d_1 - d_2$ ) 0.033.



observed at RT and 650 °C. After yielding (point  $a_1$  on the blue line in Fig. 4), the intergranular crack was firstly observed shown in Fig. 7a2. And no slip lines around the crack were observed. As the strain increased to 0.014 (point  $b_1$  on the blue line in Fig. 4), more intergranular cracks were observed, and slip bands appeared in grain interior and passed through carbides, as shown in Fig. 7b1. In addition, the carbides (marked by yellow arrows) were not cracking, although slip bands slipped through them, which is different from that at RT. Meanwhile, the first crack

further propagated in width and depth, and the crack tip had shifted to the adjacent grain boundary shown in Fig. 7b2. As the strain further increased to 0.02, it can be seen that the intergranular cracks coalesced to form macrocracks along the grain boundaries (indicated by white dotted line) from Fig. 7c1 and c2. The observations of fractured surface are shown in Fig. 7( $d_1 - d_3$ ), some shallow dimples and intergranular cracks were observed on the cross section of fractured surface in Fig. 7d2 and d3, respectively, which indicating a mixed mode of transgranular and

**Figure 6** In-situ tensile deformation process at 650 °C under strain levels: ( $a_1 - a_2$ ) 0.01, ( $b_1 - b_2$ ) 0.016, ( $c_1 - c_2$ ) 0.021, and ( $d_1 - d_2$ ) 0.026.

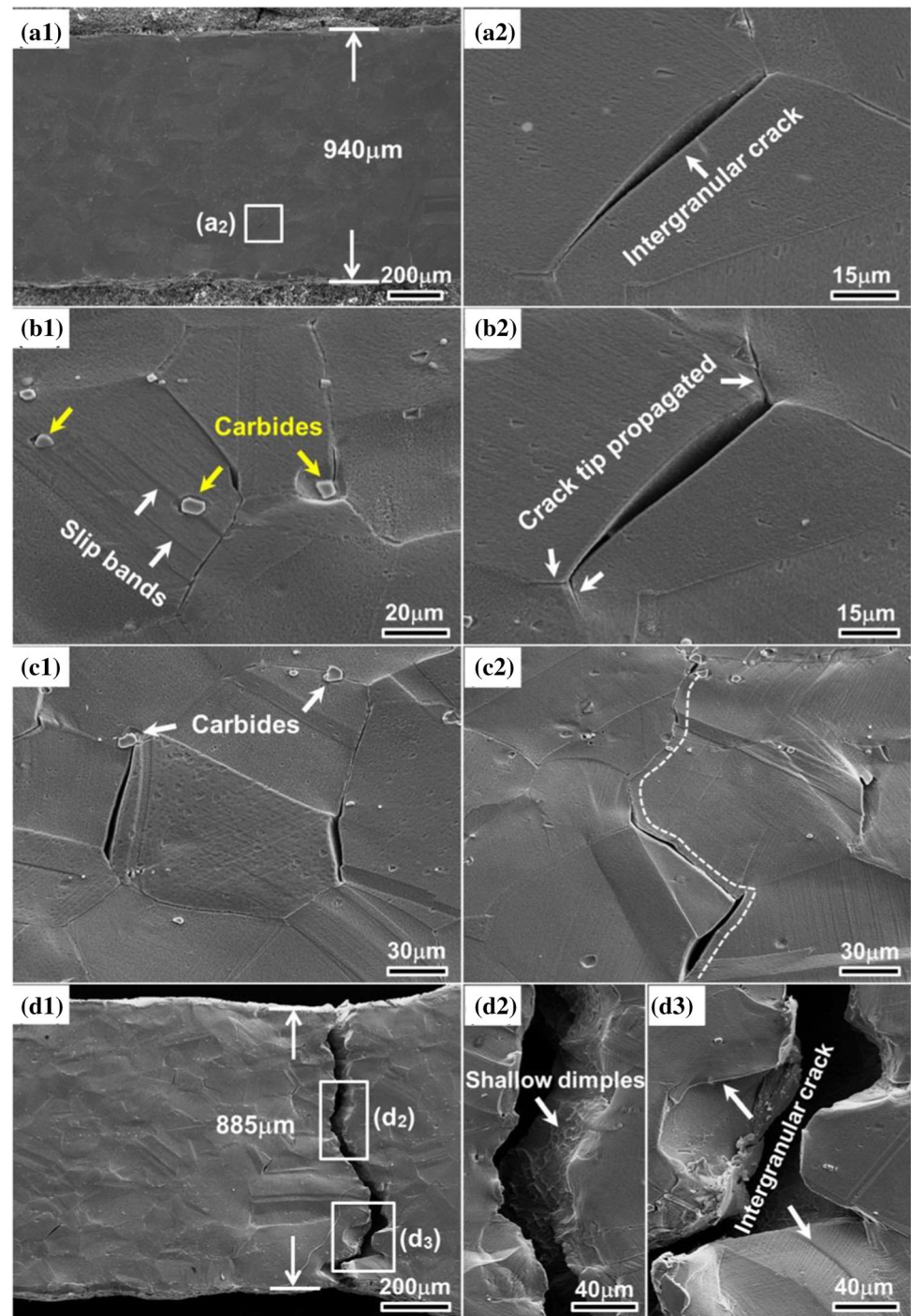


intergranular fracture. The longitudinal length decreases from 940 (Fig. 7a1) to 885 μm (Fig. 7d1), and the longitudinal strain is 5.8%, revealing that the necking is not obvious compared to that at RT. This is consistent with the results of lower elongation and reduction of cross section at 750 °C in Table 2.

**SEM fractographies at RT, 650 °C and 750 °C**

Figure 8 shows the overall fracture surface of IN718 specimens after uniaxial tensile tests at RT, 650 °C and 750 °C. Figure 8a shows the fractograph of the specimen after tensile at RT. It can be seen that the fracture surface is covered by many equiaxed dimples indicating that a ductile transgranular fracture mode. Moreover, some discrete voids can be

**Figure 7** In-situ tensile deformation process at 750 °C under strain levels: ( $a_1 - a_2$ ) 0.011, ( $b_1 - b_2$ ) 0.014, ( $c_1 - c_2$ ) 0.02, and ( $d_1 - d_2$ ) 0.024.



observed on the surface. The fracture surface at 650 °C is comparable to that at RT, as shown in Fig. 8b. The surface characterized by a mixed structure of equiaxed dimples and shallow dimples along the shear regions as shown in the area (marked by the yellow square), which indicated that the fracture mode belongs to a transgranular ductile fracture. However, the fracture surface at 750 °C shown in

Fig. 8c is obviously different from that at RT and 650 °C. It exhibits typical mixed fracture characteristics: There are many shallow dimples indicated by white arrows on the transgranular ductile surface, while a number of intergranular cracks are indicated by yellow arrows on the fracture surface, which reveal that the final failure is a combination of both trans- and intergranular fracture mode at 750 °C.



**Figure 8** Comparison of fracture surfaces of IN718 specimens after tensile tests at a RT, b 650 °C and c 750 °C.

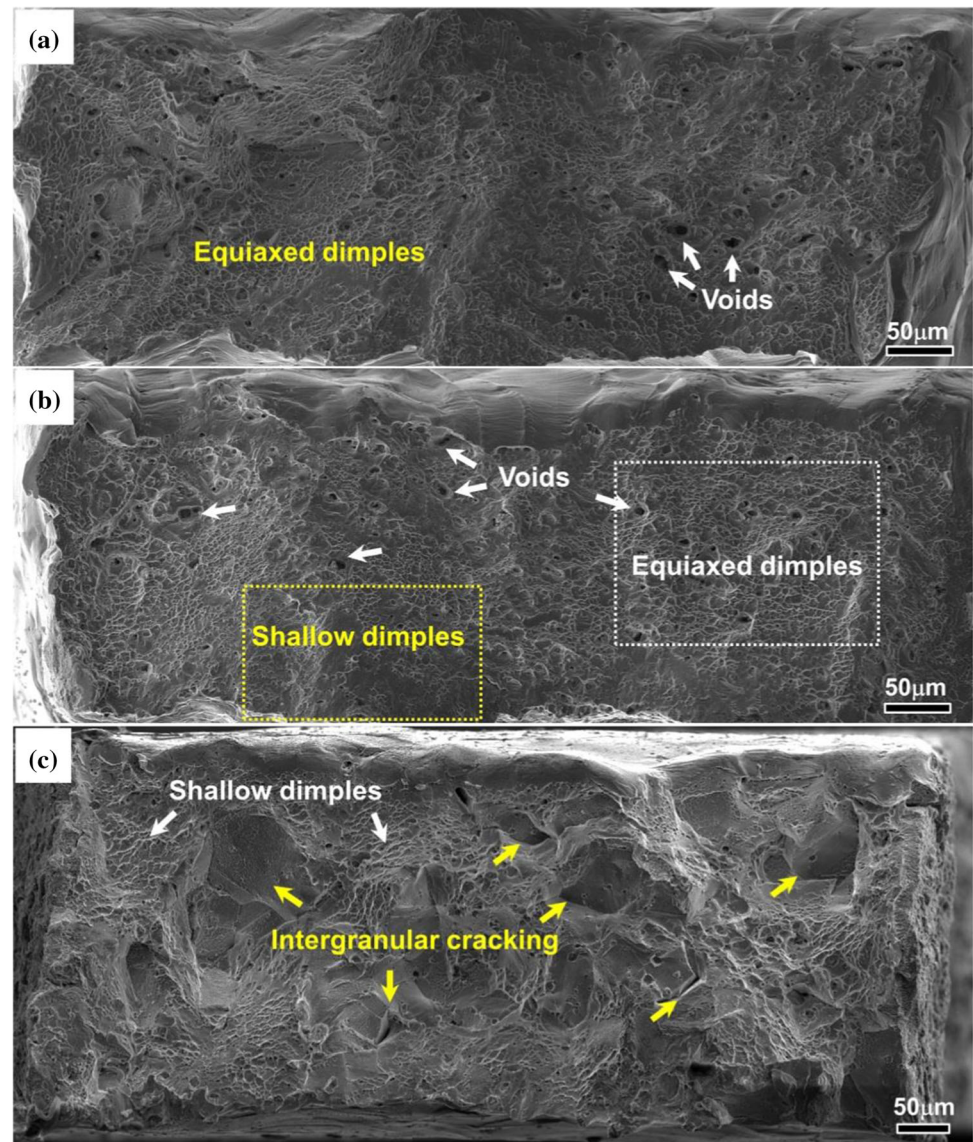
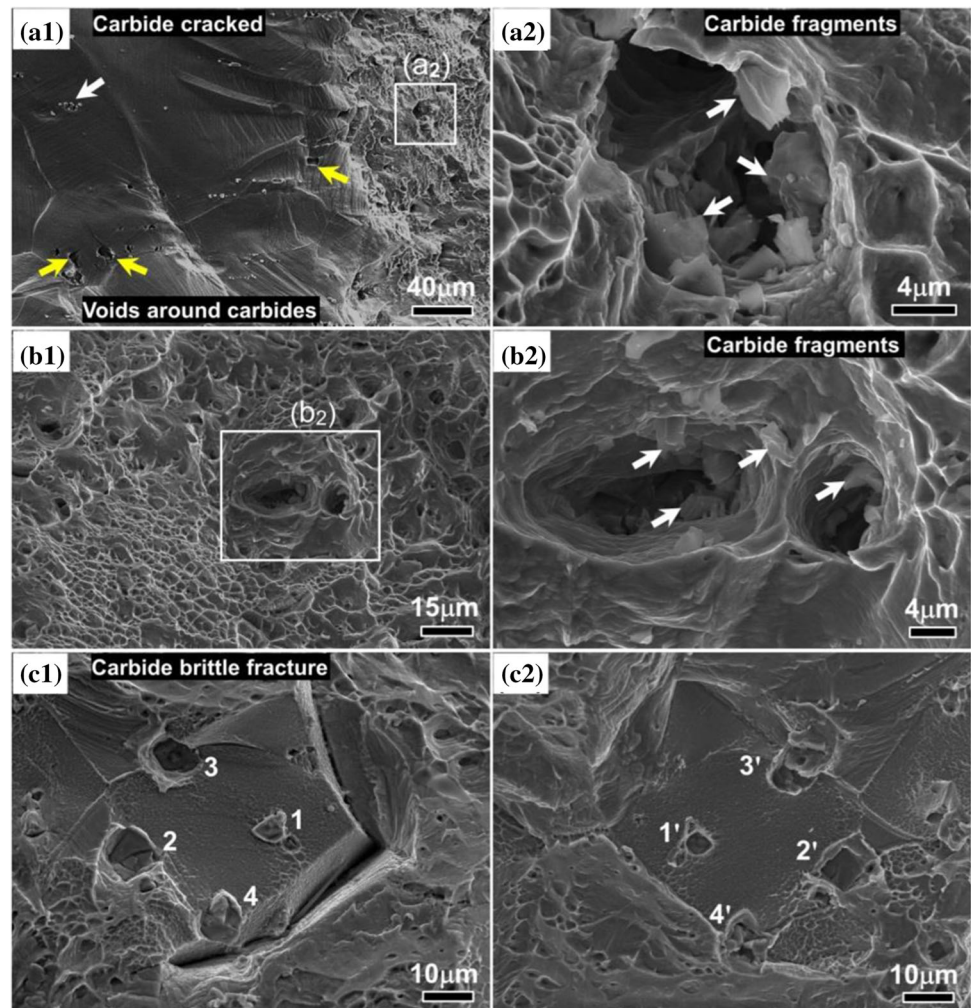


Figure 9 shows the carbide morphologies on fracture surface after tensile tests at RT, 650 °C and 750 °C. Some broken carbides marked by white arrow can be clearly observed on the surface near the fracture surface shown in Fig. 9a1, which indicated that the carbides cracking occurred during loading before failure. The voids marked by yellow arrows can also be found around the broken carbides, which were caused by the interfacial debonding of  $\gamma$  matrix and carbides [26]. A typical void microstructure feature with some carbide fragments is shown in Fig. 9a2. At 650 °C, the similar void morphologies are shown in Fig. 9b1 and b2. Carbide fragments distribute on the walls of voids as shown in Fig. 9b2. However, the

fracture morphology of carbides at 750 °C is different from that at RT and 650 °C. Figure 9c1 and c2, respectively, exhibits the fracture morphologies on both sides of the four carbides on the fracture surface denoted by the same numbers. It is found that the fracture surfaces of these carbides are neat and flat, and no carbide fragments is observed, indicating that carbides do not break into pieces before failure, but directly brittle fracture accompanied by the fracture of specimen. This is consistent with the observations in Fig. 7b1 and c1.

**Figure 9** SEM images showing carbides on fracture surface of IN718 specimens after tensile tests at ( $a_1 - a_2$ ) RT, ( $b_1 - b_2$ ) 650 °C and ( $c_1 - c_2$ ) 750 °C.



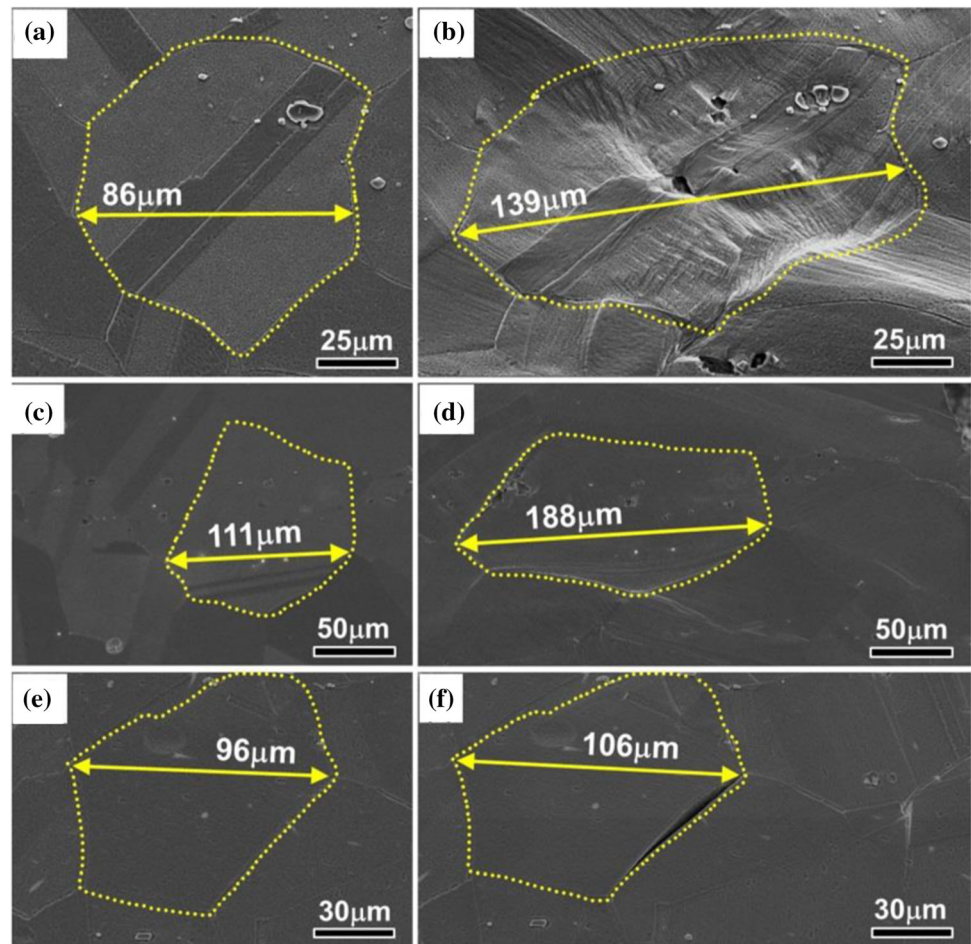
### Comparison of tensile deformation behaviors

Based on the results above, it can be found that the deformation behavior at RT is similar to that at 650 °C and quite different from that at 750 °C. To better clarify the effect of temperature on the tensile deformation behaviors, Fig. 10 shows a comparison of the grain elongations marked by yellow dotted lines near the fracture before and after tensile tests at the three temperatures. The grains are significantly stretched along the tensile direction and the elongations at RT and 650 °C are 62% and 69%, respectively, as shown in Fig. 10a, b and c, d. Although the shape of grain boundary changes with the deformation of grains, it remains intact. While at 750 °C, the grain elongation is markedly reduced to 10%, and the cleavage of grain boundary occurs, as shown in Fig. 10e, f. These

observations also support the ductility results shown in Table 2.

Another obvious deformation feature is the way of crack initiation and propagation. Figure 11 compares the behavior of crack initiation and propagation during tensile tests at the three temperatures. It can be seen that cracks initiate preferentially where dense slip bands accumulate and tangle, such as the interface of  $\gamma$  matrix/carbides (Fig. 11a) or triple junctions of grain boundaries (Fig. 11c). Subsequently, these cracks connect with each other and propagate in a transgranular manner (Fig. 11b and d) at RT and 650 °C. However, cracks primarily initiate at grain boundaries when temperature increases to 750 °C (Fig. 11e), and then propagate in an intergranular manner (Fig. 11f).

**Figure 10** Comparison of the elongation of grains near fracture surface before and after tensile tests at **a, b** RT, **c, d** 650 °C and **e, f** 750 °C.



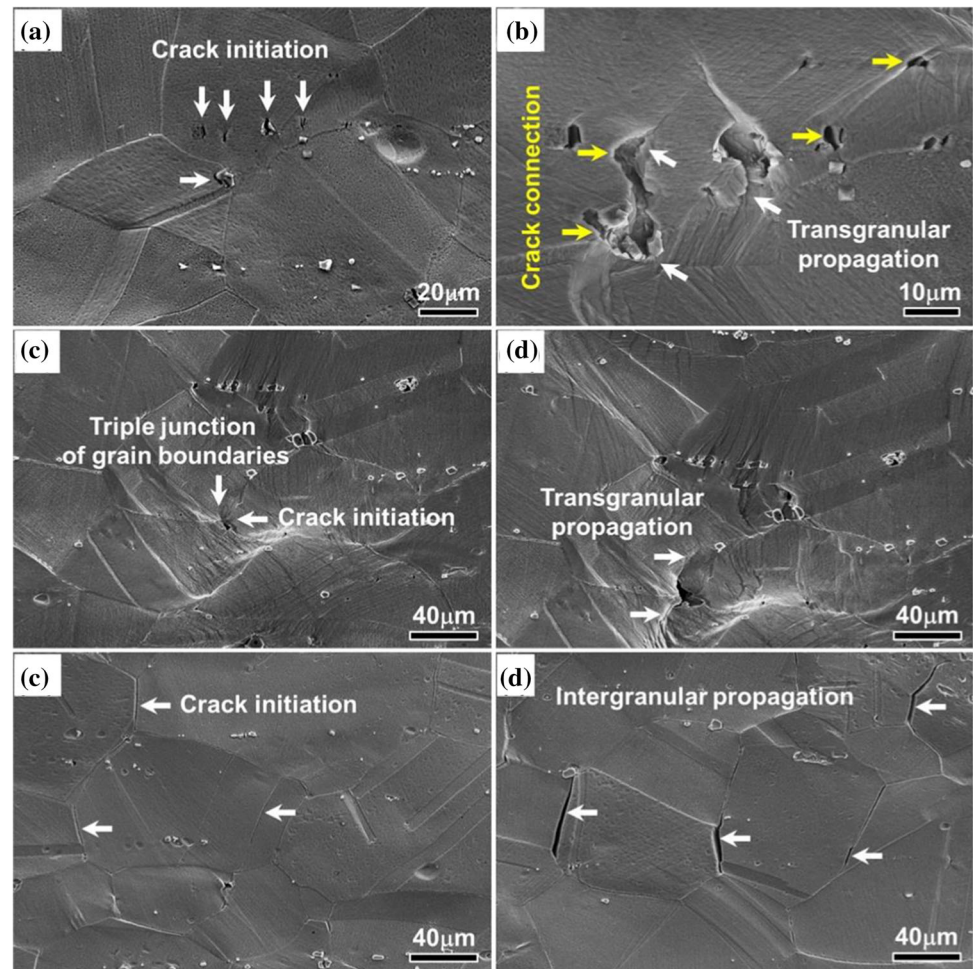
## Discussion

### Effect of temperature on tensile deformation behaviors

According to the results above, it can be concluded that temperature has a strong influence on the tensile deformation behaviors of IN718 alloy. This is attributed to the pronounced mismatch of the strength between grain interior and grain boundary at different temperatures [27]. Previous studies [28–30] reveal that the grain boundary strength is higher than intragranular strength under low temperature in polycrystalline alloys. Therefore, grain boundaries are difficult to deform during plastic deformation at low temperature ( $T < 0.5T_m$ ), and would act as strong dislocation barriers [31]. Besides, the large carbides are generally considered as dislocation motion obstacles [26, 32]. During plastic deformation, the dislocations would be impeded at the interface of  $\gamma$  matrix/carbides and ahead of grain boundaries. As

the strain increases, the pile-ups of dislocation lead to severe stress concentration around these regions. Once the stress concentration reaches a certain level, voids or cracks would generate (Fig. 11a, c) and then propagate in a transgranular manner through the width of the specimen (Fig. 6b2, Fig. 11b, d). Consequently, the plastic deformation is dominated by crystal slip at RT and 650 °C. This is similar to the damage micromechanism predicted by Kumar et al. [33] using Lemaitre's damage assessment methodology during tensile test at ambient temperature and 823 K. However, the limitation is that Kumar et al. only considered the influence of temperature. Through in-situ observations, it can be found that in addition to temperature, the different microstructure features are also important factors affecting the deformation mechanism, such as the size, distribution and amount of carbides, as well as the grain boundary structure. Therefore, the interaction of localized dislocations with large carbide particles and grain boundaries should be responsible for the crack

**Figure 11** Comparison of crack initiation and propagation during tensile tests at **a, b** RT, **c, d** 650 °C and **e, f** 750 °C.



initiation and propagation in present study. Similar results were also reported by several researchers in different alloys [29, 34–37].

However, as the temperature rises to 750 °C, intergranular cracks appear and propagate along grain boundaries, the tensile strength and the elongation decrease significantly compared to that at RT. This phenomenon is consistent with the intermediate temperature embrittlement of Ni-based superalloys reported by Zheng et al. [24], who discussed six interpretations through the representative investigations on intermediate temperature embrittlement of Ni and Ni-based superalloys, but no one seems to be applicable for our results. Interestingly, the intergranular cracks are observed prior to the occurrence of slip lines after over-taking yield point (Fig. 7a2). This result is similar to the results from Summers et al. [36], who reported that no slip bands were observed during tension of STAL15-CC alloys at 750 °C, and attributed this phenomenon to creep due to

dislocation climb. Liu et al. [38] revealed that the high deformation temperature and low strain rate might accelerate the dislocation motion and dislocation annihilation, and then decrease the dislocation multiplication and dislocation density. That seems to explain why the slip lines are still not observed around the intergranular crack after yielding in this study. However, unlike Ref. [36], with the increase in strain, the sparse slip bands begin to appear on the surface of grains before the final fracture, indicating that a weak plastic deformation occurred within grains. Meanwhile, it is crucial that the cohesive strength of grain boundary is greatly deteriorated due to thermal activity at high temperature [39]. As a result, the cleavage of grain boundary easily generates by the external load, leading to the formation of intergranular cracks directly. Subsequently, the cracks propagate rapidly along the grain boundaries, resulting in a low ductility of specimen.

Another interesting finding is the cracking behavior of carbides during tensile tests. A number of studies [17–19, 26, 36, 39, 40] have reported that the large carbides were sheared into fragments due to the interactions with dense slip bands at low temperatures. It is well known that the carbide is hard brittle phase and cannot coordinate deformation with grains [19]. As the stress reaches the break limit of carbides, the carbides cracking occurs [26]. Moreover, the carbide fragments can be observed on the walls of voids within the fracture (Fig. 9a2 and b2), indicating a serious plastic deformation around carbides before the final fracture, which is consistent with the SEM observations on the surface of the specimens (Fig. 11b, d). By contrast, the cracking of carbides at 750 °C is not observed until the final fracture of specimen, which suggests that deformation temperature significantly affect the cracking behavior of carbides. On the one hand, the stress concentration around carbides is greatly reduced due to the decrease of dislocation density caused by the high temperature [38]. On the other hand, before the stress concentration reaches the break limit of carbides, the grain boundaries cleavage preferentially at elevated temperature (Fig. 7a2), thus further releasing the stress around the carbides. Therefore, the carbides located on the grain boundary do not break into pieces before failure, but directly brittle fracture accompanied by the intergranular fracture of specimen, which can be evidenced by the fractured carbides with smooth surface distributed on the fracture surface (Fig. 9c1 and c2), and no fragments are observed.

### Effect of temperature on fracture mechanisms

According to the dense equiaxed dimples on the fracture surface (Fig. 8a, b), it can be determined that the fracture mode is a typical transgranular ductile fracture at RT and 650 °C. However, the fracture is covered with large amounts of intergranular cracks and some shallow dimples at 750 °C (Fig. 8c), which indicate a dominant intergranular brittle fracture with some degree of ductile fracture. This shift from trans- to intergranular fracture can be believed to be responsible for the decrease in strength and ductility [41].

According to Rho [42], the competition between intergranular and transgranular fracture mode is

influenced by temperature in FCC metals. It seems to be similar to what is known in polycrystalline alloys that intergranular cracking dominates above a critical temperature, i.e., so-called iso-strength temperature  $T_s$  at which the grain and grain boundary have equal strength. For IN718 alloys, the strength of grain boundary is relative high compared to the intragranular strength at low temperatures (less than or equal to 650 °C). As a result, the grain is preferentially deformed by crystal slip, and transgranular cracking is preferred. However, both intragranular strength and grain boundary strength decrease at high temperatures (greater than  $T_s$ ), especially the grain boundary strength decreases more rapidly due to the increase of grain boundary activity. Hence, grain boundary cleavage or sliding is the main deformation mechanism and leads to intergranular fracture. The similar conclusion was also reported by Ma et al. [43]. This phenomenon can be schematically demonstrated in Fig. 12. Accordingly, the  $T_s$  for IN718 alloy can be deduced as between 650 and 750 °C in present study. It should be noted that the microstructure does not change with the increase of temperature because the tensile is a short time loading process, so only the influence of temperature on tensile deformation behavior was considered in this study. Therefore, the model shown in Fig. 12 may be not accountable for the macroscopic deformation mechanism of IN718 alloy during long-term service.

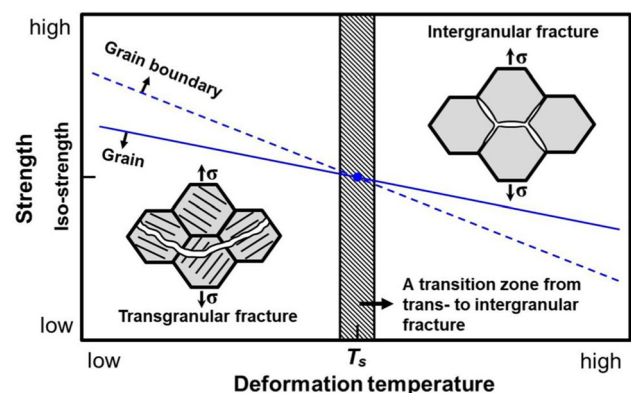


**Figure 12** Schematic diagram of the relationship between deformation temperature and fracture mode.

## Conclusions

The tensile deformation behaviors of IN718 were investigated in detail using a novel in-situ high-temperature tensile testing device at RT, 650 °C and 750 °C.

1. From RT to 650 °C, the YS and UTS keep a relatively high level due to the dominant strain hardening. The necking occurs during plastic deformation at both temperatures, especially at RT. While at 750 °C, the YS and UTS decrease significantly because of serious deterioration of the grain boundary strength. The elongation and reduction of cross section also show a significant decrease from RT to 750 °C, caused by the intermediate temperature embrittlement phenomenon.
2. During tensile tests at RT and 650 °C, the crack mainly occurs near carbide particles and triple junction of grain boundary, and then propagates in transgranular manner. Meanwhile, carbide cracking is observed during plastic deformation, but no intergranular crack is formed. At 750 °C, cracks initiate at grain boundary and propagate in an intergranular manner. No carbide cracking occurs during the whole deformation process. It suggests that the local stress around carbides at 750 °C is obviously lower than the stress level required for carbide cracking.
3. The influences of deformation temperature on the fracture mechanism are significant. At RT and 650 °C, the tensile deformation is dominated by dislocation movement and crystal slip, and the fracture mode is a typical transgranular ductile fracture. Whereas at 750 °C, a large amounts of intergranular cracks are observed on surface during tension, and the fracture microstructures are characterized by lots of intergranular cracks and some shallow dimples, which reveals a combination of both trans- and intergranular fracture mode at 750 °C.

## Acknowledgements

This research was funded by Basic Science Center Program for Multiphase Media Evolution in Hypergravity of the National Natural Science Foundation of

China (No. 51988101) and Key Projects of Beijing Natural Science Foundation (KZ202110005006).

## Declarations

**Conflict of Interest** The authors declare that they have no conflict of interest.

## References

- [1] Dehmas M, Lacaze J, Niang A, Viguier B (2011) TEM study of high-temperature precipitation of delta phase in Inconel 718 alloy. *Adv Mater Sci Eng* 2011:1–9
- [2] Radhakrishna C, Rao KP (1997) The formation and control of Laves phase in superalloy 718 welds. *J Mater Sci* 32:1977–1984. <https://doi.org/10.1023/A:1018541915113>
- [3] Zhang HJ, Li C, Liu YC, Guo QY, Li HJ (2016) Precipitation behavior during high temperature isothermal compressive deformation of Inconel 718 alloy. *Mater Sci Eng A* 677:515–521
- [4] Chamanfar A, Sarrat L, Jahazi M, Asadi M, Weck A, Koul AK (2013) Microstructural characteristics of forged and heat treated Inconel-718 disks. *Mater Des* 52:791–800
- [5] Zhang HJ, Li C, Liu YC, Guo QY, Huang Y, Li HJ, Yu JX (2017) Effect of hot deformation on  $\gamma''$  and  $\delta$  phase precipitation of Inconel 718 alloy during deformation and isothermal treatment. *J Alloy Compd* 716:65–72
- [6] Chen YT, Yeh AC, Li MY, Kuo SM (2017) Effects of processing routes on room temperature tensile strength and elongation for Inconel 718. *Mater Des* 119:235–243
- [7] Zhang HJ, Li C, Guo QY, Ma ZQ, Huang Y, Li HJ, Liu YC (2018) Hot tensile behavior of cold-rolled Inconel 718 alloy at 650 °C: the role of  $\delta$  phase. *Mater Sci Eng A* 722:136–146
- [8] Kitaguchi H (2012) Microstructure-property relationship in advanced Ni-based superalloys. *Metallurgy - Advances in Materials and Processes*, pp 20–21. <https://doi.org/10.5772/52011>
- [9] Oradei-Basile A, Radavich J (1991) Superalloys 718, 625, and various derivatives. In: *Proceedings of the Minerals Metals and Materials Society*, Pittsburgh. pp 325–335
- [10] Desvalle'es Y, Bouzidi M, Bois F, Beaude N, Loria EA (1994) Superalloy 718-metallurgy and applications, minerals, metals and materials society. Warrendale, PA 7:281–291
- [11] Warren J, Wei DY (2006) The cyclic fatigue behavior of direct age 718 at 149, 315, 454, and 538 °C. *Mater Sci Eng A* 428:106–115
- [12] Rai AK, Tripathy HP, Hajra RN, Raju S, Saibaba S, Jayakumar T (2016) Measurement of high temperature phase

- stability and thermophysical properties of alloy 740. *Mater Sci Technol* 32:488–497
- [13] Zhao SQ, Xie XS, Smith GD, Patel SJ (2003) Microstructural stability and mechanical properties of a new nickel-based superalloy. *Mater Sci Eng A Struct Mater Prop Microstruct Process* 355:96–105
- [14] Zhao YS, Zhang J, Song FY, Zhang M, Luo YS, Zhao H, Tang DZ (2020) Effect of trace boron on microstructural evolution and high temperature creep performance in Re-containing single crystal superalloys. *Prog Nat Sci Mater Int* 30:371–381
- [15] Liu BB, Han JQ, Zhao R, Liu W, Wan M (2016) Grain size effect on fracture behavior of the axis-tensile test of Inconel 718 sheet. *High Temp Mater Proc* 35:989–998
- [16] Wang Y, Shao WZ, Zhen L, Yang C, Zhang XM (2009) Tensile deformation behavior of superalloy 718 at elevated temperatures. *J Alloys Compd* 471:331–335
- [17] Lin YC, Deng J, Jiang YQ, Wen DX, Liu G (2014) Hot tensile deformation behaviors and fracture characteristics of a typical Ni-based superalloy. *Mater Des* 55:949–957
- [18] Zhao R, Li XJ, Wan M, Han JQ, Meng B, Cai ZY (2017) Fracture behavior of Inconel 718 sheet in thermal-aided deformation considering grain size effect and strain rate influence. *Mater Des* 130:413–425
- [19] Lu XD, Du JH, Deng Q (2013) In situ observation of high temperature tensile deformation and low cycle fatigue response in a nickel-base superalloy. *Mater Sci Eng A* 588:411–415
- [20] Andersson H, Persson C (2004) In-situ SEM study of fatigue crack growth behavior in IN718. *Int J Fatigue* 26:211–219
- [21] Boehlert CJ, Li H, Wang L (2010) Slip system characterization of Inconel 718 using in-situ scanning electron microscopy. *Adv Mater Process* 41–45
- [22] Ma JY, Lu JX, Tang L, Wang J, Sang LJ, Zhang YF, Zhang Z (2020) A novel instrument for investigating the dynamic microstructure evolution of high temperature service materials up to 1150 °C in scanning electron microscope. *Rev Sci Instrum* 91:043704
- [23] Lu JX, Chang L, Wang J, Sang LJ, Wu SK, Zhang YF (2018) In-situ investigation of the anisotropic mechanical properties of laser direct metal deposition Ti6Al4V alloy. *Mater Sci Eng A* 712:199–205
- [24] Zheng L, Schmitz G, Meng Y, Chellali R, Schlesiger R (2012) Mechanism of intermediate temperature embrittlement of Ni and Ni-based Superalloys. *Crit Rev Solid State and Mater Sci* 37:181–214
- [25] Sheng LY, Yang F, Guo JT, Xi TF (2014) Anomalous yield and intermediate temperature brittleness behaviors of directionally solidified nickel-based superalloy. *Trans Nonferrous Metal Soc* 24:673–681
- [26] Zhang SH, Zhang HY, Cheng M (2011) Tensile deformation and fracture characteristics of delta-processed Inconel 718 alloy at elevated temperature. *Mater Sci Eng A* 528:6253–6258
- [27] Rao GA, Kumar M, Srinivas M, Sarma DS (2003) Effect of standard heat treatment on the microstructure and mechanical properties of hot isostatically pressed superalloy Inconel 718. *Mater Sci Eng A* 355:114–125
- [28] Palumbo G, Aust KT (1995) Solute effects in grain boundary engineering. *Canad Metall Q* 34:165–173
- [29] Wang J, Zhang YF, Ma JY, Li JX, Zhang Z (2017) Microcrack nucleation and propagation investigation of Inconel 740H alloy under in situ high temperature tensile test. *Acta Metall Sin* 53:1627–1635
- [30] Lin YC, Li L, He DG, Chen MS, Liu GQ (2017) Effects of pre-treatments on mechanical properties and fracture mechanism of a nickel-based superalloy. *Mater Sci Eng A* 679:401–409
- [31] Chaturvedi MC, Han YF (1983) Strengthening mechanisms in Inconel 718 superalloy. *Met Sci* 17:145–149
- [32] Du BN, Hu ZY, Sheng LY, Cui CY, Yang JX, Zheng YF, Sun XF (2018) Tensile, creep behavior and microstructure evolution of an as-cast Ni-based K417G polycrystalline superalloy. *J Mater Sci Tech* 34:1805–1816
- [33] Kumar J, Kumar A, Kumar V (2011) Ambient and high temperature in situ damage evolution in nickel based IN 718 superalloy. *Mater Sci Eng A* 528:4009–4013
- [34] Zhang WJ, Song XY, Hui SX, Ye WJ (2017) In-situ SEM observations of fracture behavior of BT25y alloy during tensile process at different temperature. *Mater Des* 116:638–643
- [35] Wang J, Lu JX, You XX, Ullah RF, Sang LJ, Chang L, Zhang YF, Zhang Z (2019) In-situ comparison of deformation behavior at 23 °C and 650 °C of laser direct melting deposited Ti–6Al–4V alloy. *Mater Sci Eng A* 749:48–55
- [36] Summers WD, Alabort E, Kontis P, Hofmann F, Reed RC (2016) In-situ high-temperature tensile testing of a polycrystalline nickel-based superalloy. *Mater High Temp* 33:338–345
- [37] Wang ZY, Wu SC, Kang GZ, Li H, Wu ZK, Fu YN, Withers PJ (2021) In-situ synchrotron X-ray tomography investigation of damage mechanism of an extruded magnesium alloy in uniaxial low-cycle fatigue with ratchetting. *Acta Mater* 211:116881
- [38] Liu ZG, Li PJ, Xiong LT, Liu TY, He LJ (2017) High-temperature tensile deformation behavior and microstructure evolution of Ti55 titanium alloy. *Mater Sci Eng A* 680:259–269
- [39] Li XF, Zhang J, Fu QQ, Akiyama E, Song XL, Wang YF, Li QZ, Zou N (2018) Tensile mechanical properties and fracture

- behaviors of nickel-based superalloy 718 in the presence of hydrogen. *Int J Hydrog Energy* 43:20118–20132
- [40] Hrutkay K, Kaoumi D (2014) Tensile deformation behavior of a nickel based superalloy at different temperatures. *Mater Sci Eng A* 599:196–203
- [41] Alabort E, Barba D, Sulzer S, LiBner M, Petrinic N, Reed RC (2018) Grain boundary properties of a nickel-based superalloy: characterisation and modeling. *Acta Mater* 151:377–394
- [42] Rho BS, Nam SW, Xie X (2002) The effect of test temperature on the intergranular cracking of Nb-A<sub>2</sub>86 alloy in low cycle fatigue. *J Mater Sci* 37:203–209. <https://doi.org/10.1023/A:1013147319646>
- [43] Ma XF, Shi HJ, Gu JL (2010) In-situ scanning electron microscopy studies of small fatigue crack growth in recrystallized layer of a directionally solidified superalloy. *Mater Lett* 64:2080–2083

**Publisher's Note** Springer Nature remains neutral with regard to jurisdictional claims in published maps and institutional affiliations.